Laser Photonics Rev. **7,** No. 1, 109–113 (2013) / **DOI** 10.1002/lpor.201200036

LASER & PHOTONICS REVIEWS

Abstract The coupled-resonator-induced transparency (CRIT) effect in parallel-coupled double microring resonators (MRRs) has been widely studied, and various applications based on the CRIT have been demonstrated. As an application of the CRIT, we propose and demonstrate a directed logic circuit that can implement the XOR and XNOR operations. Two electrical signals applied to the two MRRs represent the two operands of the logical operations, and the operational results are represented by the output optical signal. As a proof-of-concept, the thermo-optic modulating scheme is employed with an operational speed of 10 kbps.

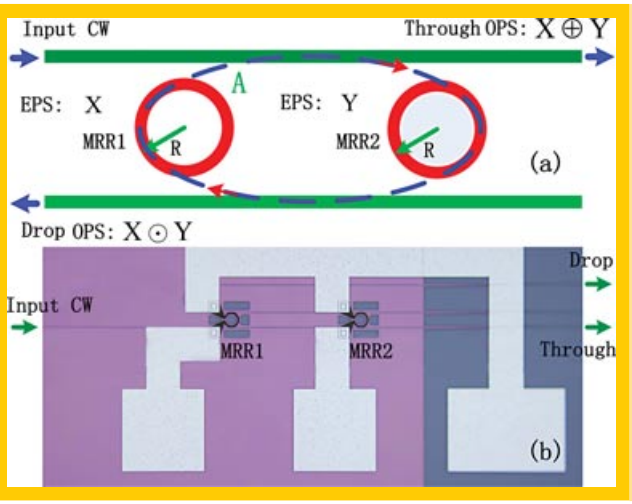

ORIGINAL PAPER

XOR/XNOR directed logic circuit based on coupled-resonator-induced transparency

Yonghui Tian[1], Lei Zhang[1], Qianfan Xu[2], and Lin Yang[1,*]

1. Introduction

Electromagnetically induced transparency (EIT) exploits the destructive quantum interference to make a medium transparent over a narrow spectral range [1–5]. Currently, various studies about EIT are done in atomic systems [1–5] and semiconductor nanostructures [6, 7]. Due to the inherent nature of EIT, various applications of EIT have been proposed and demonstrated such as controlling photons [3], light storage [5], and slow light [8]. Recent theoretical analyses and experimental demonstrations have revealed that the photonic analog to EIT phenomenon known as coupled-resonator-induced transparency (CRIT) can be observed in a coupled resonator system due to the coherent interference between the two resonance pathways [9–14]. In addition, various applications based on CRIT have been demonstrated such as storing light [15–17], slow light [18], and wavelength routing [19].

Compared to electrical computing, optical computing has many advantages such as high modulation speed, high parallelism, and low latency [20, 21]. It is well known that the fundamental optical logic gates form the basic building blocks to perform complex logic operations in optical computing [22]. Generally, there are two ways to achieve some fundamental logical operations. One way is to exploit the material nonlinear effect to achieve all-optical logic operations. Indeed, this way can perform high-speed operations. However, it needs a strong pump light to generate the nonlinear effect to perform operations [23]. Therefore, it is difficult to achieve a large-scale integration on a single chip. The other way is to exploit a novel logic scheme to perform logic operations. For example, directed logic proposed by Hardy and Shamir in 2007 [20] has been shown to be very suitable for optical computing. Directed logic is a novel logic paradigm that employs the optical switch network to perform the logic operations. Electrical signals representing the operands of the operations control the state of each optical switch in the network and the operation results are output at the output ports in the form of light. The operation of each switch is independent of others and all switches perform their operations simultaneously. Therefore, their switching delays do not accumulate—in contrast to electronic logic circuits wherein gate delays are cascaded, resulting in large latency [20, 24]. Microring resonator (MRR) is very suitable to act as the switching element of the directed logic due to its compact size, low power consumption and high response speed. Currently, various directed logic circuits based on microring resonators (MRRs) have been proposed and demonstrated [24–27]. In this letter, we demonstrate a directed logic circuit that can perform the XOR and XNOR logical operations based on the CRIT (XOR and XNOR represent exclusive-OR and exclusive-NOR, respectively).

[1] State Key Laboratory on Integrated Optoelectronics, Institute of Semiconductors, Chinese Academy of Sciences Beijing 100083, China
[2] Department of Electrical and Computer Engineering, Rice University, Houston Texas 77005, USA
*Corresponding author(s): e-mail: oip@semi.ac.cn

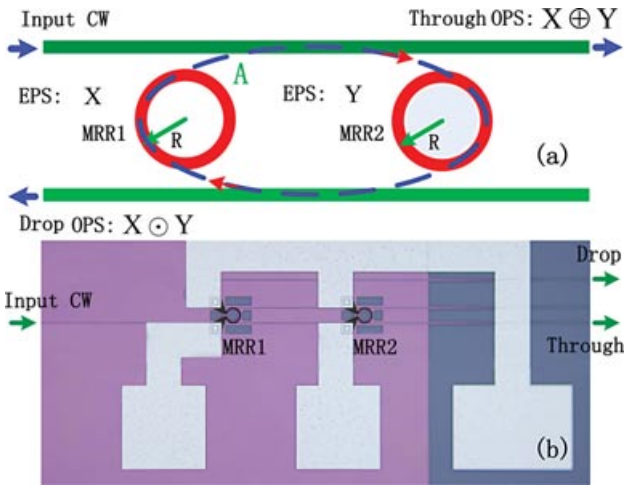

Figure 1 (online color at: www.lpr-journal.org) (a) Architecture and (b) micrograph of the device (CW: continuous wave, EPS: electrical pulse trains, OPS: optical pulse trains, MRR: microring resonator). The blue dashed line represents the closed cavity formed by two coupled microring resonators.

2. Architecture and principle

The proposed architecture consisting of a pair of microring resonators coupled with two parallel waveguides is schematically shown in Fig. 1a. Monochromatic continuous optical wave with the working wavelength of λ_w is coupled into the input port, and then modulated by two electrical signals X and Y that tune the resonances of two MMRs in the CRIT structure. We regard X and Y as a sequence of Boolean digital signal, where 0 and 1 are represented by the low and high levels of an electrical pulse, respectively. The optical pulse trains at the through and drop ports represent the final results of XOR and XNOR operations of the two operands X and Y, respectively. A logic 1 state is achieved when the optical power at the output port is at the high level, and a logic 0 state is achieved when the optical power at the output port is at the low level.

The through-port transmission spectrum of the CRIT has a narrow peak in the center of the broad dip when the two MRRs have similar resonances due to the constructive interference between the two MRRs. Correspondingly, the spectrum at the drop port shows a narrow dip in the center of the broad peak. The narrow peak and dip disappear and the light is confined in the closed cavity (shown as the blue dashed line in Fig. 1a) when the two MRRs have the same resonances [10]. In order to describe the principle of the device, we first explain the physical reason of the transparency peak. We regard the system shown in Fig. 1a as a Fabry−Pérot cavity and the two MRRs as two planar mirrors. Then we can obtain the transmission and reflection spectra of the Fabry−Pérot cavity at the through and drop ports. According to coupled mode theory, the normalized transmission can be written as follows [28, 29],

$$|T(\lambda)|^2 = \frac{|t_1(\lambda)t_2(\lambda)|^2}{(1-|r_1(\lambda)r_2(\lambda)|)^2} \times \frac{1}{1+4\left(\frac{\sqrt{|r_1(\lambda)r_2(\lambda)|}}{1-|r_1(\lambda)r_2(\lambda)|}\right)^2 \sin^2\frac{\varphi(\lambda)}{2}} \quad (1)$$

where $t_{1,2}(\lambda)$ and $r_{1,2}(\lambda)$ represent the amplitude transmission and reflection coefficients for MRR1 and MRR2 and can be expressed as follows [3].

$$t_{1,2}(\lambda) = \frac{j(2\pi c/\lambda - 2\pi c/\lambda_{1,2}) + \gamma^{\mathrm{i}}_{1,2}}{j(2\pi c/\lambda - 2\pi c/\lambda_{1,2}) + \left(\gamma^{\mathrm{i}}_{1,2} + \gamma^{\mathrm{c}}_{1,2}\right)} \quad (2)$$

$$r_{1,2}(\lambda) = \frac{-\gamma^{\mathrm{c}}_{1,2}}{j(2\pi c/\lambda - 2\pi c/\lambda_{1,2}) + \left(\gamma^{\mathrm{i}}_{1,2} + \gamma^{\mathrm{c}}_{1,2}\right)}. \quad (3)$$

Here, $\lambda_{1,2}$ are the resonance wavelengths of MRR1 and MRR2. γ^{i} is the intrinsic loss coefficient, which is related to the intrinsic quality factor Q_{int} by $\gamma^{\mathrm{i}} = \pi c/Q_{\mathrm{int}}\lambda_0$. γ^{c} is the waveguide-cavity coupling coefficient, which is related to the coupling quality factor Q_{c} by $\gamma^{\mathrm{c}} = \pi c/Q_{\mathrm{c}}\lambda_0$. $\varphi(\lambda)$ is the round-trip phase accumulated in the waveguides (shown as the blue dashed line in Fig. 1a). $|T(\lambda)|^2$ is maximized when $\varphi(\lambda)$ is a multiple of 2π, which means that the light experiences constructive interference in the Fabry−Pérot cavity. In this condition, the transmission spectrum at the through port exhibits a narrow symmetric transparency peak centered on a wavelength of λ_{tr}. The center-to-center distance between the two MRRs is $4\pi R$, where R represents the radius of the MRR. The radius of R is specially designed so that $\varphi(\lambda_{\mathrm{tr}})$ is close to a multiple of 2π [10, 19]. For simplicity, we assume that the two MRRs are intrinsically lossless, and they have the same coupling rate to a waveguide, which means $\gamma^{\mathrm{i}}_{1,2} = 0$ and $\gamma^{\mathrm{c}}_{1,2} = \gamma$($\gamma^{\mathrm{i}}_{1,2}$and $\gamma^{\mathrm{c}}_{1,2}$represent the intrinsic loss coefficient and waveguide−cavity coupling coefficient for MRR1 and MRR2, respectively). Therefore, when $\lambda = \lambda_{tr}$, Eq. (1) can be simplified as follows,

$$|T(\lambda_{tr})|^2 = \frac{|t_1(\lambda_{tr})t_2(\lambda_{tr})|^2}{(1-|r_1(\lambda_{tr})r_2(\lambda_{tr})|)^2}, \quad (4)$$

where

$$t_{1,2}(\lambda_{tr}) = \frac{j(2\pi c/\lambda_{tr} - 2\pi c/\lambda_{1,2})}{j(2\pi c/\lambda_{tr} - 2\pi c/\lambda_{1,2}) + \gamma} \quad (5)$$

$$r_{1,2}(\lambda_{tr}) = \frac{-\gamma}{j(2\pi c/\lambda_{tr} - 2\pi c/\lambda_{1,2}) + \gamma}. \quad (6)$$

Coherent interaction between the two MRRs occurs only when the two MRRs have similar resonance wavelengths [13]. When the detuning between the two resonance

wavelengths of the two MRRs is large, the two MRRs cannot be coupled mutually, and the narrow transparency peak disappears. When the two MRRs have the same resonance wavelengths, the transparency peak also disappears since the reflection coefficients $r_{1,2}$ are equal to -1 (Eq. (6), which means that light is completely confined in the closed cavity (shown as the blue dashed line in Fig. 1a). Therefore, the normalized transmission $|T(\lambda)|^2$ and the optical power directed to the through port can be tuned by changing the resonances of the MRRs, which means that the high and low levels of the optical power (logic states 1 and 0) can be achieved at the through port. Here, we only analyze the performance of the device at the through port. The performance of the device at the drop port can be analyzed in a similar way except that the transparency peak is replaced by the transparency dip.

When the wavelength of the light is aligned with the transparency peak, the XOR and XNOR operations can be achieved at the through and drop ports of the device, respectively. The initial state is defined as follows. The voltages applied to the MRRs are at the low level (X = 0, Y = 0), and the two MRRs have the same resonance wavelength at the initial state. Therefore, no transparency peak occurs in the center of the broad dip at the initial state, and the light is directed to the drop port and the optical power is at the low level at the through port (logic state 0). When one of two voltages applied to the MRRs is at the high level (X = 0, Y = 1 or X = 1, Y = 0), a detuning between the two resonances of the MRRs is formed and the transparency peak appears at the input light wavelength of λ_w, the light is directed to the through port and the optical power is at the high level at the through port (logic state 1). When the voltages applied to the two MRRs are both at the high level (X = 1, Y = 1), the resonances of the two MRRs shift to the longer wavelength and the transparency peak disappears at its original location and the light is directed to the drop port and the optical power is at the low level at the through port (logic state 0).

3. Device fabrication

The device is fabricated on an eight-inch silicon-on-insulator wafer with a 2-μm thick buried dioxide layer and a 220-nm top silicon layer. The micrograph of the device is shown in Fig. 1b. The straight and ring waveguides are defined by 248-nm deep ultraviolet (UV) photolithography, and formed by inductively coupled plasma etching. The waveguide is 400 nm in the width, 220 nm in the height and 70 nm in the slab thickness. The radius of the MRR is 10 μm and the gap between the ring waveguide and the straight waveguide is 275 nm. After the waveguides are fabricated, 1.5-μm thick SiO_2 is deposited on the top of the waveguides as a separate layer, and then two TiN microheaters with the width of 2 μm and the thickness of 120 nm are fabricated on the top of the ring waveguides. Al traces with the width of 50 μm are formed to connect the microheaters and the pads. A thermo-optic modulating scheme is adopted for proof-of-concept since it demands a less-complex device layer structure and consequently yields easier fabrication steps.

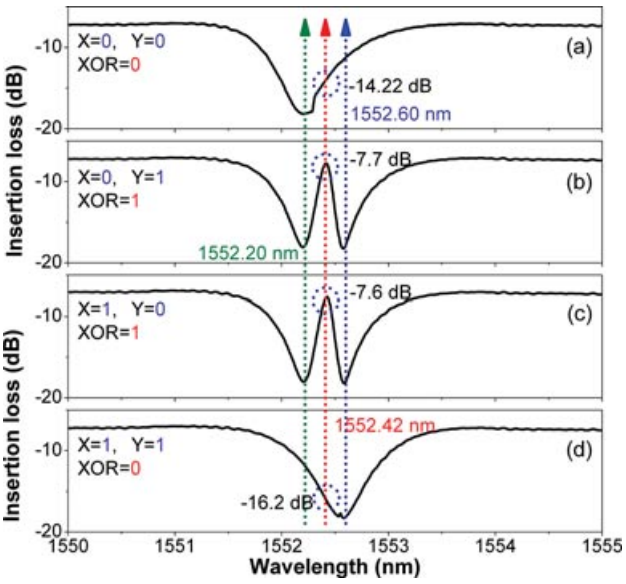

Figure 2 (online color at: www.lpr-journal.org) Static response at the through port with the voltages applied to MRR1 and MRR2 being (a) 0.48 and 0 V, (b) 0.48 and 0.93 V, (c) 1.00 and 0 V, (d) 1.00 and 0.93 V.

4. Experimental result

In order to determine the working wavelength of λ_w and the analog working voltages of the device, the static response spectra of the device is measured as follows. An amplified spontaneous emission source (ASE), two tunable voltage sources and an optical spectrum analyzer (OSA) are employed to characterize the static response of the device. The broadband light is coupled into the input port through a lensed fiber, and the output light is fed into the OSA through another lensed fiber. Two tunable voltage sources are employed to drive two microheaters on the top of the MRRs. When the MRRs are heated up, the effective refractive index of the ring waveguides increases and the resonances of the MRRs shift to longer wavelengths. The static response spectra at the through port are shown in Fig. 2. The two MRRs are designed to have the same physical parameters. However, the resonances of the two MRRs are slightly different due to the limited fabrication accuracy. A 0.48-V pre-bias voltage is applied to MRR1 and no voltage is applied to MRR2 in order to offset the fabrication error and let the two MRRs have the same resonance wavelength of 1552.20 nm at the initial state (X = 0, Y = 0 (Fig. 2a). According to Eqs. (4)–(6), we can change the resonances of the MRRs to change the transmission and reflection coefficients of the MRRs and the possible maximum transmission power. We assume that the working wavelength of λ_w locates at the narrow transparency peak of 1552.42 nm in the static response spectra of the

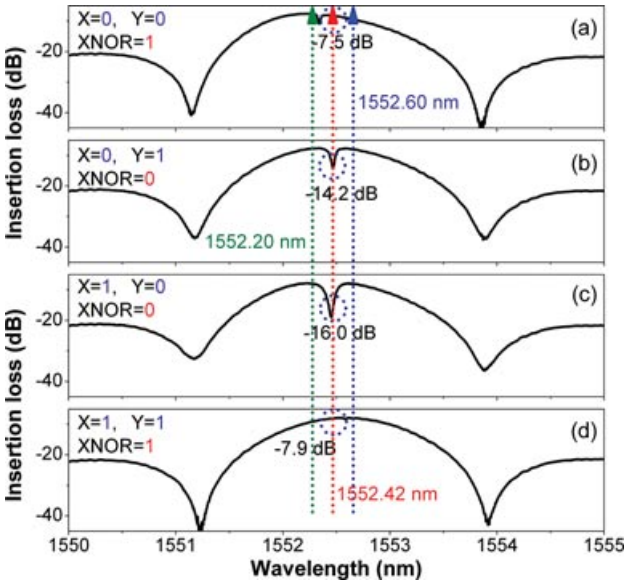

Figure 3 (online color at: www.lpr-journal.org) Static response at the drop port with the voltages applied to MRR1 and MRR2 being (a) 0.48 and 0 V, (b) 0.48 and 0.93 V, (c) 1.00 and 0 V, (d) 1.00 and 0.93 V.

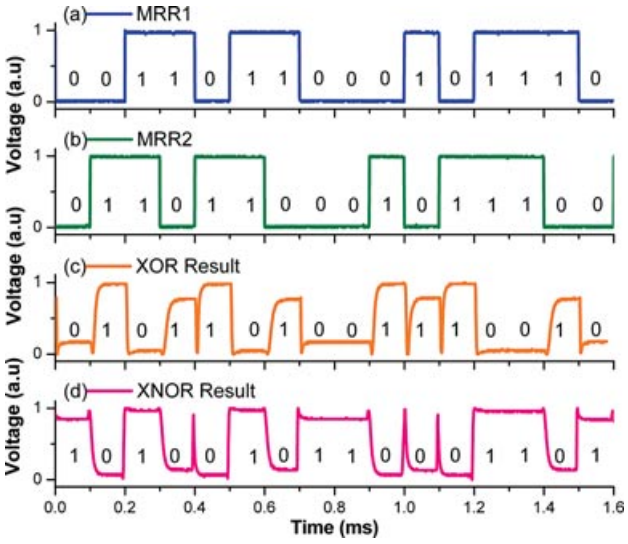

Figure 4 (online color at: www.lpr-journal.org) Signals applied to (a) MRR1 and (b) MRR2, (c) XOR operation result at the through port and (d) XNOR operation result at the drop port.

device (Fig. 2), and the output optical power is at the low level (logic state 0) at the initial state (X = 0, Y = 0 (Fig. 2a). The MRR2's resonance shifts from 1552.20 nm to 1552.60 nm and the MRR1's resonance does not change when the voltages applied to MRR1 and MRR2 are 0.48 V and 0.93 V (Fig. 2b). The MRR1's resonance shifts from 1552.20 to 1552.60 nm and the MRR2's resonance does not change when the voltages applied to MRR1 and MRR2 are 1 V and 0 V (Fig. 2c). The transparency peak at the λ_w can appear in the two logic states since a small detuning between the resonances of the two MRRs is formed and the two MRRs have similar resonance wavelengths, and the output optical power at the through port is at the high level (logic state 1). The resonances of the two MRRs shift from 1552.20 nm to 1552.60 nm when the voltages applied to MRR1 and MRR2 are 1 V and 0.93 V, respectively (Fig. 2d). The transparency peak at the λ_w disappears since the resonances of the MRRs shift to the right of the λ_w (Fig. 2d), and the optical power at the through port is at the low level (logic state 0).

The static response spectra at the drop port in all four logic states are shown in Fig. 3. The four logic states at the through port of the device are characterized with the transparency peak. In fact, the transparency peaks in Fig. 2 correspond to the transparency dips in Fig. 3 one by one. Therefore, the same process used for the static response spectra at the through port can be employed to discuss the static response spectra at the drop port of the device.

The dynamic response of the device is shown in Fig. 4. A monochromatic light at the λ_w from a tunable laser is coupled into a polarization rotator and then is coupled into the input port of the device. Two binary sequences non-return-to-zero signals at 10 kbps are applied to MRR1 and MRR2, respectively. (The low levels are 0.48 V and 0 V for MRR1 and MRR2, respectively. The high levels are 1 V and 0.93 V for MRR1 and MRR2, respectively.) The output light is transformed to an electrical signal by a photodetector. All the four input and output electrical signals are fed into a four-channel oscilloscope for waveform observation. From Fig. 4, we can see clearly that the XOR and XNOR operation of the two electrical signals are achieved at the through and drop ports, respectively. Some small sharp dips and peaks can be found in Figs. 4c and d, which originate from the transition of the different operation states. Similar phenomena have also been observed in other directed logic circuits and the detailed discussion can be found in our previous paper [30].

5. Conclusion

In conclusion, we have proposed and demonstrated a directed logic circuit that can implement the XOR/XNOR logical operations using CRIT. The final operation results are obtained at the through and drop ports in the form of the light. As a proof of concept, a thermo-optic modulation scheme is employed with an operation speed of 10 kbps. Recently, MRR-based optical switches with a high-speed modulation scheme have been proposed and demonstrated [31–36]. In fact, all these advanced modulation schemes such as the carrier-depletion modulation and the electric-field effects can be applied to the proposed circuit to achieve higher-speed operation.

Acknowledgements. This work has been supported by the National Natural Science Foundation of China (NSFC) under grants 61235001, 60977037, 61204061 and 61205008, and by the National High Technology Research and Development Program of China under grant 2012AA012202.

Received: 10 June 2012, **Revised:** 21 October 2012, **Accepted:** 22 October 2012

Published online: 13 December 2012

Key words: Coupled-resonator-induced transparency, microring resonator, directed logic, silicon waveguide, XOR/XNOR operation.

References

[1] K.-J. Boiler, A. Imamoglu, and S. E. Harris, Phys. Rev. Lett. **66**(20), 2593–2596 (1991).
[2] S. E. Harris, Phys. Today **50**(7), 36–42 (1997).
[3] M. D. Lukin and A. Imamoglu, Nature **413**(6853), 273–276 (2001).
[4] M. D. Eisaman, A. Andre, F. Massou, M. Fleischhauer, A. S. Zibrov, and M. D. Lukin, Nature **438**(7069), 837–841 (2005).
[5] D. F. Phillips, A. Fleischhauer, A. Mair, R. L. Walsworth, and M. D. Lukin, Phys. Rev. Lett. **86**(5), 783–786 (2001).
[6] M. Phillips, H. Wang, I. Rumyantsev, N. H. Kwong, R. Takayama, and R. Binder, Phys. Rev. Lett. **91**(18), 183602–183605 (2003).
[7] M. Phillips and H. Wang, Opt. Lett. **28**(10), 831–833 (2009).
[8] L. V. Hau, S. E. Harris, Z. Dutton, and C. H. Behroozi, Nature **397**(6720), 594–598 (1999).
[9] D. D. Smith, H. Chang, K. A. Fuller, A. T. Rosenberger, and R.W. Boyd, Phys. Rev. A **69**(6), 063804(1–6) (2004).
[10] Q. Xu, S. Sandhu, M. L. Povinelli, J. Shakya, S. Fan, and M. Lipson, Phys. Rev. Lett. **96**(12), 123901(1–4) (2006).
[11] S. T. Chu, B. E. Little, W. Pan, T. Kaneko, and Y. Kokebun, IEEE Photon. Technol. Lett. **11**(11), 1426–1428 (1999).
[12] L. Maleki, A. B. Matsko, A. A. Savchenkov, and V. S. Ilchenko, Opt. Lett. **29**(6), 626–628 (2004).
[13] A. Melloni, Opt. Lett. **26**(12), 917–919 (2001).
[14] Y. Zhang, S. Darmawan, L. Y. M. Tobing, T. Mei, and D. H. Zhang, J. Opt. Soc. Am. B **28**(1), 28–36 (2011).
[15] Q. Xu, P. Dong, and M. Lipson, Nature Phys. **3**(6), 406–410 (2007).
[16] L. Yosef Mario and M. K. Chin, Opt. Exp. **16**(3), 1796–1807 (2008).
[17] J. B. Khurgin, J. Opt. Soc. Am. B **22**(5), 1062–1074 (2005).
[18] K. Totsuka, N. Kobayashi, and M. Tomita, Phys. Rev. Lett. **98**(21), 213904(1–4) (2006).
[19] M. Mancinelli, R. Guider, P. Bettotti, M. Masi, M. R. Vanacharla, and L. Pavesi, Opt. Exp. **19**(13), 12227–12240 (2011).
[20] J. Hardy, and J. Shamir, Opt. Exp. **15**(1), 150–165 (2007).
[21] L. Yang, R. Q. Ji, L. Zhang, J. J. Ding, and Q. Xu, Opt. Exp. **20**(12), 13560–13565 (2012).
[22] C. Qiu, X. Ye, R. Soref, L. Yang, and Q. Xu, Opt. Lett. **37**(19), 3942–3944 (2012).
[23] Q. Xu, and M. Lipson, Opt. Exp. **15**(3), 924–929 (2007).
[24] Q. Xu, and R. Soref, Opt. Exp. **19**(6), 5244–5259 (2011).
[25] R. Soref, Adv. Optoelectron. Article ID 627802, doi:10.1155/2011/627802(2011)
[26] L. Zhang, R. Q. Ji, L. X. Jia, L. Yang, P. Zhou, Y. H. Tian, P. Chen, Y. Y. Lu, Z. Y. Jiang, Y. L. Liu, Q. Fang, and M. B, Yu, Opt. Lett. **35**(10), 1620–1622 (2010).
[27] Y. H. Tian, L. Zhang, R. Q. Ji, Lin Yang, and Q. Xu, Opt. Lett. **36**(19), 3795–3797 (2011).
[28] J. Pan, Y. Huo, S. Sandhu, N. Stuhrmann, M. L. Povinelli, J. S. Harris, M. M. Fejer, and S. Fan, Appl. Phys. Lett. **97**(10), 101102(1–3) (2010).
[29] B. E. A. Saleh, and M. C. Teich, Fundamentals of Photonics (Wiley, New York, 1991), Chap. 9.
[30] Y. H. Tian, L. Zhang, R. Q. Ji, L. Yang, P. Zhou, H. T. Chen, J. F. Ding, W. W. Zhu, Y. Y. Lu, L. X. Jia, Q. Fang, and M. B. Yu, Opt. Lett. **36**(9), 1650–1652 (2011).
[31] S. Sandhu and S. H. Fan, Opt. Exp. **20**(4), 4280–4290 (2012).
[32] W. D. Sacher and J. K. S. Poon, Opt. Exp. **16**(20), 15741–15753 (2008).
[33] T. Ye and X. Cai, J. Lightwave Technol. **28**(11), 1615–1623 (2010).
[34] A. S. Liu, L. Liao, D. Rubin, H. Nguyen, B. Ciftcioglu, Y. Chetrit, N. Izhaky, and M. Paniccia, Opt. Exp. **15**(2), 660–668 (2007).
[35] M. Hochberg, T. Baehr-Jones, G. Wang, M. Shearn, K. Harvard, J. Luo, B. Chen, Z. Shi, R. Lawson, P. Sullivan, A. K. Jen, L. Dalton, and A. Scherer, Nature Mater. **5**(9), 703–709 (2006).
[36] C. Koos, P. Vorreau, T. Vallaitis, P. Dumon, W. Bogaerts, R. Baets, B. Esembeson, I. Biaggio, T. Michinobu, F. Diederich, W. Freude, and J. Leuthold, Nature Photon. **3**(4), 216–219 (2009).